J. R. Gibson
A. J. Dow
Canada Centre For Remote Sensing
Ottawa, Ontario K1A OY7, Canada
S. E. Masry
Surveying Engineering Department
University of New Brunswick
Fredericton, N.B. E3B 5A3, Canada

Adjustment of Position Using Inertial Navigation Systems

Clusters of ground targets spaced at appropriate flying time intervals are used to correct the errors of the inertial navigation system in post-flight processing.

Abstract: *Preliminary results from a system comprised of an inertial navigation system and an aerial camera which are hard mounted together indicate that position estimates may be obtained which are in error by no more than 2.2 metres (1σ confidence limit). The system which has been developed by the Canada Centre for Remote Sensing in conjunction with the Department of Surveying Engineering of the University of New Brunswick for the Canadian Hydrographic Service, was originally conceived to complement water-borne hydrographic charting procedures in shallow water areas.*

Clusters of ground targets spaced at appropriate flying time intervals are used to correct the errors of the inertial navigation system in post-flight processing, thereby enabling highly accurate position estimates for those photographs which do not contain ground targets. Thus, the system is ideally suited for coastal mapping where complete ground control coverage would be very expensive and often impractical. Also, the system has good potential for conventional photogrammetric mapping projects where ground control targets could be set in clusters at appropriate intervals.

Introduction

The positioning results described in this paper have been obtained from a system comprised of an inertial navigation system and an aerial camera which are rigidly connected together. The system has been developed for the Canadian Hydrographic Service by the Canada Centre for Remote Sensing and the Department of Surveying Engineering of the University of New Brunswick to prove the concept of using an inertial navigation system and an aerial camera to provide data for coastal mapping and water depth measurement in shallow water. The design criterion was to provide highly accurate position and attitude data at the time of each camera firing in order to enable the subsequent formation of stereo models with an analytical plotter.

System Description

The system, known as the Photo Hydrography System, consists of an airborne subsystem (Figure 1) for gathering data and a ground subsystem (Figure 2) for post flight data processing.

The airborne subsystem consists of

- RC-10 aerial survey camera,
- LTN-51 inertial navigation system (INS),
- Barometric altimeter, and
- Airborne Data Acquisition System (ADAS).

The ground based subsystem consists of

- PDP-10 data processing system (CCRS) and
- Analytical Plotter (University of New Brunswick).

The inertial navigation system provides position and attitude data during flight. The ADAS monitors

Photogrammetric Engineering and Remote Sensing,
Vol. 47, No. 2, February 1981, pp. 185-192.

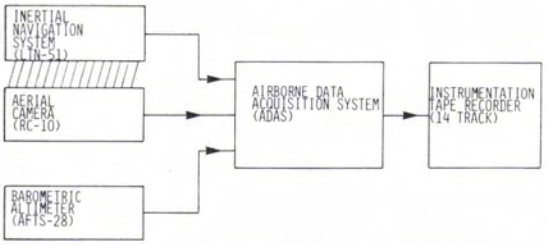

FIG. 1. Airborne data collection subsystem.

and records pertinent information during the flight. This includes time, navigation data, and camera firings. The flight lines of the aircraft are chosen to pass over preselected areas where accurately surveyed ground control targets have been placed. This is shown schematically in Figure 3. The post-flight data processing consists of determining the camera position and attitude by photogrammetric resection for those photos that contain the ground targets and using this information to correct the navigation data supplied by the inertial and other systems. Thus corrected, the position and attitude data for the remaining photos that do not contain targets may be used in an analog or analytical plotter to provide information for forming stereo models. For measuring water depth, an analytical plotter is preferable in order to take into account the refraction of light at the air-water interface (Masry, 1972). The effects of the instability of the air-water interface on the accuracy of the photogrammetrically measured water depths must also be considered. These details are beyond the scope of this paper and have been dealt with elsewhere (Masry, 1978).

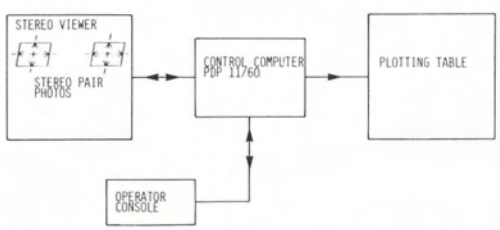

FIG. 2. Ground based photogrammetric processing subsystem.

POSITIONING RESULTS

The balance of this paper deals with the positioning results that have been obtained from a series of test flights flown over the U.S. Defense Mapping Agency's Photogrammetric Test Range at Casa Grande, Arizona. A previous paper (Masry *et al.*, 1978) has discussed the preliminary results of the attitude subsystem. Since the publication of that paper, the data processing techniques have continued to evolve. The purpose of this paper is to present the results from a very simple and effective position data processing algorithm that uses cubic splines as a means of interpolating between photofix measurement points.

MATHEMATICAL DEVELOPMENT

The inertial navigation system (INS) does not calculate position information directly, but indirectly by propagating position changes through a direction cosine matrix (DCM). The DCM defines the rotation from Earth fixed axes (X_e, Y_e, Z_e in Figure 4) to the INS platform axes (X_p, Y_p, Z_p) and is represented symbolically by $\boldsymbol{C}_e^p$. The order of rotation is as follows: λ (Longitude) about the X_e axis, ψ (latitude) about the once displaced Y_e axis, and $\propto$ (wander angle) about the twice displaced Z_e axis. The complete expression for $\boldsymbol{C}_e^p$ is given by

$$\boldsymbol{C}_e^p = \begin{pmatrix} \cos\propto\cdot\cos\psi & \sin\propto\cdot\cos\lambda + \cos\propto\cdot\sin\lambda\cdot\sin\psi & \sin\propto\cdot\sin\lambda - \cos\propto\cdot\cos\lambda\cdot\sin\Psi \\ -\sin\propto\cdot\cos\psi & \cos\propto\cdot\cos\lambda - \sin\propto\cdot\sin\lambda\cdot\sin\psi & \cos\propto\cdot\sin\lambda + \sin\propto\cdot\cos\lambda\cdot\sin\psi \\ \sin\psi & -\sin\lambda\cdot\cos\psi & \cos\lambda\cdot\cos\psi \end{pmatrix}$$

As the INS moves about on the ellipsoid, the elements of the DCM must change to reflect the changing angles of rotation. The matrix $\dot{\boldsymbol{C}}_e^p$, representing the time derivative of the DCM, is given by (Britting, 1971, p. 16)

$$\dot{\boldsymbol{C}}_e^p = \boldsymbol{\Omega} \cdot \boldsymbol{C}_e^p \tag{1}$$

where $\boldsymbol{\Omega}$ is a skew symmetric matrix of angular velocities expressed in INS platform coordinates,

$$\boldsymbol{\Omega} = \begin{pmatrix} 0 & \rho_z & -\rho_y \\ -\rho_z & 0 & \rho_x \\ \rho_y & -\rho_x & 0 \end{pmatrix} \tag{2}$$

The terms ρ_x, ρ_y, and ρ_z are angular velocities about the X_p, Y_p, and Z_p axes, respectively. The platform of the INS is maintained at local level at all times so that the accelerations sensed along the X_p and Y_p axes will not contain any gravity component. The x and y accelerations are measured, corrected for Coriolis effects, and then integrated

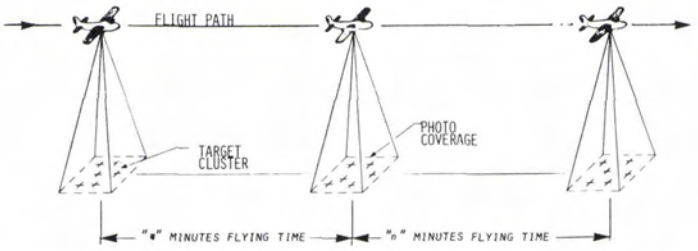

FIG. 3. Schematic diagram showing idealized flight line with clusters of ground targets spaced at "n" minute flying time intervals.

to give the velocity components, V_x and V_y. The angular velocities, ρ_x and ρ_y, required for the matrix $\boldsymbol{\Omega}$, may then be obtained from V_x and V_y and the Earth radius components in the $Y_p - Z_p$ and $X_p - Z_p$ planes, and are given by

$$\rho_x = \frac{-V_y}{R_y} \tag{3}$$

$$\rho_y = \frac{+V_x}{R_x} \tag{4}$$

A wander azimuth mechanization was utilized in the LTN-51 INS in which the z axis is not driven, and hence $\rho_z = 0$.

The solution to Equation 1 is given by

$$\boldsymbol{C}_e^p(t) = e^{\boldsymbol{\Omega}(t)\,(t-t_0)}\,\boldsymbol{C}_e^p(t_0) \tag{5}$$

where the matrix exponential form, $e^{\mathbf{X}}$, is given by

$$e^{\mathbf{X}} = \boldsymbol{I} + \boldsymbol{X} + \frac{\boldsymbol{X}^2}{2!} + \frac{\boldsymbol{X}^3}{3!} + \ldots \tag{6}$$

Data processing in the LTN-51 is accomplished by a general purpose digital computer using integer arithmetic. Thus, a discrete time version of Equation 5 has been implemented:

$$\boldsymbol{C}_e^p(t_n) = \boldsymbol{\Phi}(t_n)\boldsymbol{C}_e^p(t_{n-1}) \tag{7}$$

where $\boldsymbol{\Phi}(t_n)$ is a single term expansion of Equation 6,

$$\boldsymbol{\Phi}(t_n) = \boldsymbol{I} + \boldsymbol{\Omega}(t_n)\Delta t,$$

$$t_n = t,\ t_{n-1} = t_0 \text{ and } \Delta t = t_n - t_{n-1}$$

Each element of the transition matrix $\boldsymbol{\Phi}(t_n)$ is shown in Equation 8. Recall that, for the particular mechanization of the LTN-51, $\rho_z = 0$. The terms containing ρ_z are shown as a matter of formality in order to fully describe the form of the matrix.

$$\boldsymbol{\Phi}(t_n) = \begin{pmatrix} 1 & \rho_z(t_n)\Delta t & -\rho_y(t_n)\Delta t \\ -\rho_z(t_n)\Delta t & 1 & \rho_x(t_n)\Delta t \\ \rho_y(t_n)\Delta t & -\rho_x(t_n)\Delta t & 1 \end{pmatrix} \tag{8}$$

The solution shown in Equation 7 with the single term expansion of $\boldsymbol{\Phi}(t_n)$ is adequate for the intended purpose of the INS. However, to use the INS in a highly accurate position determining system, there are a number of shortcomings which must be taken care of in order to obtain the required accuracy in the position information.

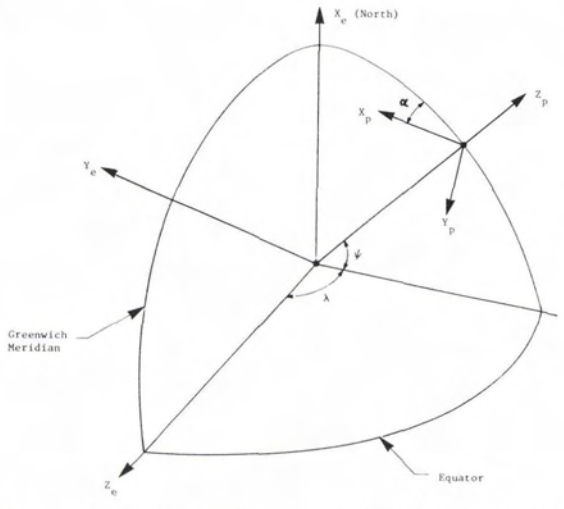

FIG. 4. Coordinate systems; Earth fixed (X_e, Y_e, Z_e) and INS platform (X_p, Y_p, Z_p).

PHYSICAL LIMITATIONS OF THE INS

There are a number of well documented shortcomings associated with inertial navigation systems in general, such as Schuler oscillations, gyro drift, accelerometer bias, scale factor errors, etc. (e.g., Britting, 1971; Broxmeyer, 1964; Savant, 1961; Benson, 1975). There is also another set of limitations to the achievable accuracies of an INS; they are introduced by the tradeoffs made in the physical implementation of the device. Specifically, the digital computer in the LTN-51 provided several examples of such tradeoffs. Since the computer is a serial bit processor without a hardware floating point unit, the algorithms developed to solve the navigation equations must maintain a very delicate balance between overall accuracy and processing time. As a result of the computational tradeoffs, neither the DCM $\boldsymbol{C}_e^p$ nor the transition matrix, $\boldsymbol{\Phi}$, are truly orthogonal. This has im-

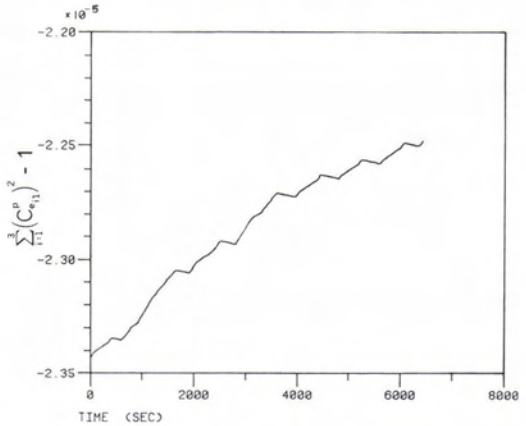

FIG. 5. Deviation from unity of the sum of squares of the elements of column 1 of the DCM from the INS computer.

plications when the elements of the DCM are used to compute latitude and longitude. Equation 9, which follows, derives from the orthogonality property of DCM's:

$$\sum_{i=1}^{3} (C^P_{e_{ij}})^2 - 1 = \epsilon_j \qquad j = 1,2,3 \tag{9}$$

Figure 5 contains a plot of ϵ_1 as a function of time for C^P_e, using data gathered directly from the LTN-51. If C^P_e were orthogonal, then the term, ϵ_1, would have a constant value of 0. It is of interest to note the growth of ϵ_1 with time; this is consistent with the unit diagonal elements of Φ. When two or more terms are employed in expanding the matrix exponential of Equation 6, the diagonal terms become less than unity and one would not expect to observe such a growth pattern. The perturbations in the trace of ϵ_1 are related to the flight path. This may be verified by comparing Figure 5 with Figures 8 and 9, One further point to consider is that, since Equation 7 is recursive, errors, once initiated, would tend to be self-sustaining. That is, there is no mechanism in the INS to bound the calculated position errors in the direct manner in which the Schuler pendulum bounds the velocity errors. Another of the implementation difficulties of the LTN-51 is that Earth radii calculations assume an altitude of sea level. This refers to the computation of R_x and R_y in Equation 3 and 4. This is not a major problem to the LTN-51; however, it does contribute to the overall errors of the device.

It was to avoid the above-mentioned difficulties that the decision was taken to reintegrate the INS velocity data in post-flight processing; that is, to make use of the capabilities of a large computer to minimize the accumulation of arithmetic errors and to optimize the correction of the systematic faults of the INS.

Error Correction Procedure

In general terms, consider the output position information from the INS as a function of time to be given by $P_I(t)$, which consists of the true position, $P_T(t)$, and an error position, $P_E(t)$:

$$P_I(t) = P_T(t) + P_E(t) \tag{10}$$

Now assuming that the true position of P_T is available at N points in time, t_i, $1 \leq i \leq N$, from photogrammetric resection data we may obtain the position error, P_E, at those N points by subtracting the true position from the INS position; thus,

$$P_E(t_i) = P_I(t_i) - P_T(t_i) \tag{11}$$

We now have a set of samples of the position error at N points in time which a simple interpolation process such as cubic splines could use to estimate the position error for other time points, t_j, where $t_1 \leq t_j \leq t_N$. To obtain the estimated true position then, the error curve generated by the cubic spline denoted by $\hat{P}_E(t)$ may be subtracted from the INS position data. Thus,

$$\hat{P}_T(t) = P_I(t) - \hat{P}_E(t) \tag{12}$$

where the symbol "^" indicates estimated values.

For projects requiring only low to medium accuracy post-flight position data, the method just described could provide acceptable results. On the other hand, considering the positional accuracies required for aerial mapping projects and the known inaccuracies of the INS numerical processes, it was evident that there was both a requirement for greater accuracy and a potential means to achieve it. Therefore, a processing scheme was devised which effectively bypassed most of the numerical problems of the LTN-51 and produced extremely accurate results.

Since the INS velocity data is in a more primitive form than that of the DCM in that it has not been directly processed in a recursive algorithm, the method developed for post-flight processing utilized the INS velocity data to re-compute the DCM (Equation 7) in a large computer. Double precision floating point arithmetic was used to minimize roundoff and truncation errors. The necessary corrections to the velocity data were generated from the derivatives of the position errors that were provided by the cubic spline interpolation function. Processing the velocity data in this way also allowed for the calibration of some of the systematic errors of the INS such as accelerometer scale factor errors and the non-orthogonalities of the INS platform axes. Another improvement realized by the post-flight ground processing was that the transition matrix, $\Phi(t_n)$, may be computed more accurately (Equations 5, 6, and 7). A three term approximation for Φ (t_n) has been used, which means that the orthogonality of the DCM will be maintained to a much better degree. Figure

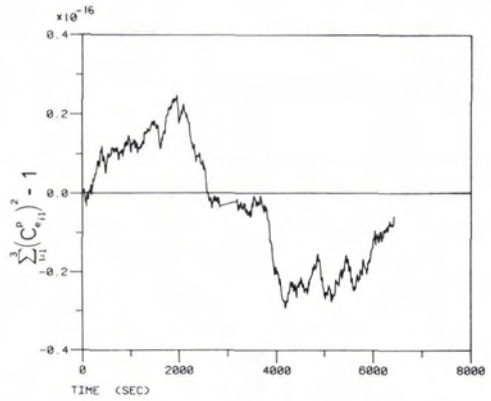

FIG. 6. Deviation from unity of the sum of squares of the elements of column 1 of the DCM from the post-flight processing program.

6 shows a plot of ϵ_1 (Equation 9) as a function of time for the ground processed $\boldsymbol{C}_e^p$. A comparison of Figures 5 and 6 shows the dramatic improvement provided by the ground processing; specifically, the term ϵ_1 from the recomputed $\boldsymbol{C}_e^p$ is 12 orders of magnitude smaller than that of the INS $\boldsymbol{C}_e^p$.

The ground processing technique is shown in schematic form in Figure 7. The procedure is iterative, with the initial set of data for calculating the velocity corrections being derived from latitude and longitude errors that are obtained by comparing INS data to photo fix data. The recomputed $\boldsymbol{C}_e^p$ is initialized using the latitude and longitude of the first photo fix and the wander angle (α) from the INS at that time. Since the original position errors of the INS were due in part to the propagation of computational errors, the first pass of the data through the process will not likely result in zero errors at the photo fix times. This is not a problem, however, because the residual errors from the first pass are simply added to the original errors and the processing is repeated. The process is judged to be complete when the residual errors at the photo fix points are less than some preselected value, say 0.1 metres. In practice, it has been found that two or three passes of the data are sufficient to achieve very high accuracy position estimates. The effect of the above process is that, by forcing the position computations through the photo fix points, the position estimates for other photo stations achieve a high degree of accuracy.

RESULTS

A series of tests were performed on one of the data sets acquired at the Casa Grande photogrammetric test range to (a) determine the maximum accuracy achievable, and (b) determine the accuracy as a function of the time interval between photo fixes. The data set consists of 105 minutes of INS data (velocity, attitude, vertical acceleration, DCM) and barometric altimeter data, all sampled at a 50 msec rate, as well as photo fix data (position, attitude) obtained from 61 photographs scattered throughout the time interval. The complete set of photos was not utilized for this study; only those photos that contained a minimum of five clearly visible ground targets were selected to ensure strong resection solutions. The flight path included a number of turns and straight segments. Plots of latitude and longitude appear in Figures 8 and 9 with dots indicating the occurrence of the 61 photographs that were used for the evaluation.

In order to assess the maximum accuracy, it was necessary to identify the minimum number of

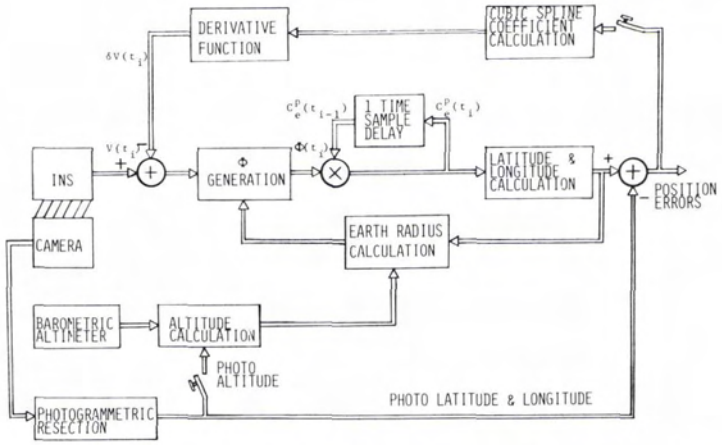

FIG. 7. Schematic diagram showing the post-flight processing. After completing each pass of data, the switches are closed to update the cubic spline interpolation function coefficients and the barometric altitude coefficients.

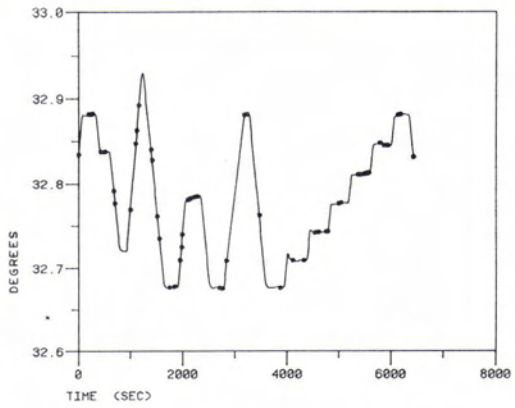

FIG. 8. Latitude data with the occurrence of each photograph marked with a dot.

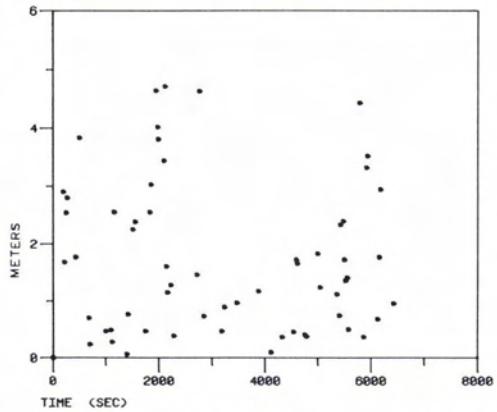

FIG. 10. The magnitude of the error vector at each photograph.

photographs required to define the straight line segments of the flight path. The reason for this is that changes in the flight path eventually show up as errors in velocity and position. The 27 photographs that defined the flight path were then used as photo fix points for the processing; the remaining 34 photographs were used to evaluate the accuracy of the system. The magnitude of the residual error vector is shown in Figure 10. The error vector consists of 3 components: (1) along track error, (2) cross track error, and (3) altitude error. Table 1 shows the 1σ error bounds of each component as well as combinations of components.

All of the residual errors are with respect to the photo fix data. That is, the photo fix data was assumed to be error free. However, the photo positions were calculated using the standard photogrammetric collinearity equations and have an estimated error magnitude of 1 metre (1σ). The ground control targets have been surveyed to first order horizontal and third order elevation standards. Future implementations of this method could be modified to account for possible errors in the photo fix data.

TABLE 1. SYSTEM ERRORS FOR FULLY DEFINED FLIGHT LINES

Error component	1σ error (m)
1 along track	1.1
2 across track	1.0
3 altitude (barometric only)	1.5
4 horizontal error (1 & 2)	1.5
5 total error (1, 2 & 3)	2.2

Figures 11 and 12 show the estimated INS error traces resolved into the platform X_p and Y_p axes. These curves were generated from the cubic spline interpolation function. The input data for the interpolation consisted of the measured errors at the photo fix points. Figures 13 and 14 show the velocity corrections derived from the position errors.

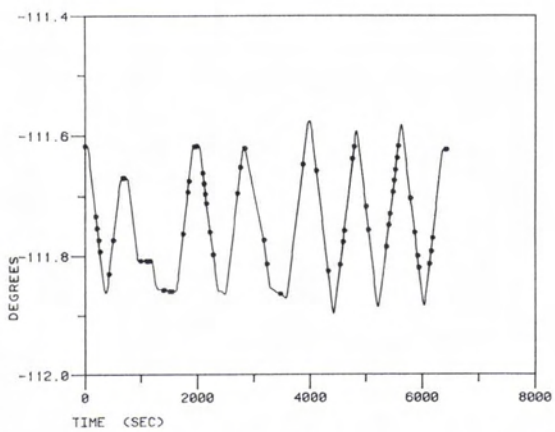

FIG. 9. Longitude data with the occurrence of each photograph marked with a dot.

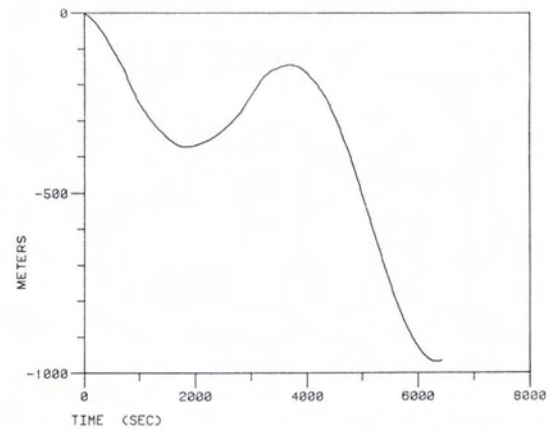

FIG. 11. The INS position error resolved along the platform X_p axis.

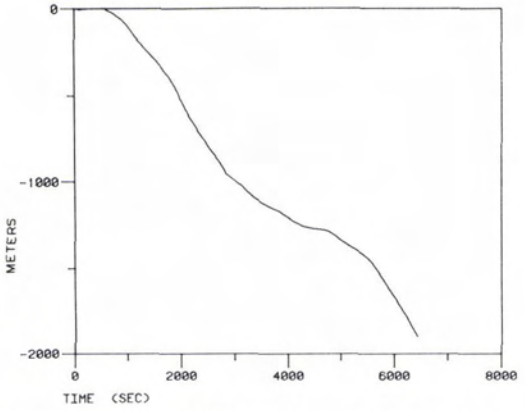

FIG. 12. The INS position error resolved along the platform Y_p axis.

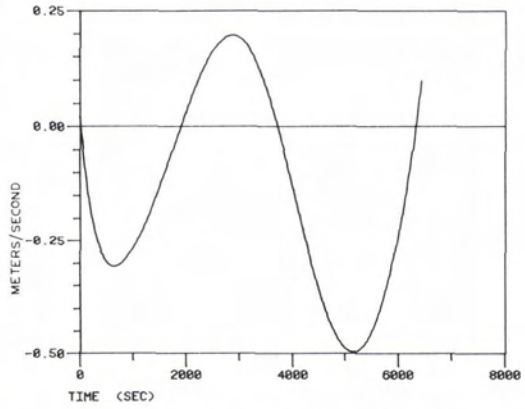

FIG. 13. The velocity correction for V_x derived from the position error along the x axis.

Following the overall evaluation, a series of tests were run with reduced numbers of photo fix points. Since the photo fix data were not spaced at regular intervals, it was not possible always to obtain the desired intervals between fixes; however, evaluations were carried out for average times between fixes of approximately 5, 10, 15, 20, and 25 minutes. Table 2 contains the 1σ error bounds of the error components for these time periods.

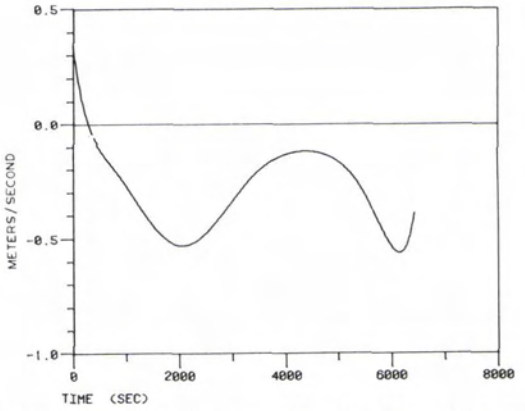

FIG. 14. The velocity correction of V_y derived from the position error along the y axis.

COMPUTING TIME

The computing for this work was done on the CCRS PDP-10 time sharing system with the majority of the programs written in Fortran. The CPU time for each test was approximately 4 minutes or 2.3 seconds per minute of data.

CONCLUSIONS

We have presented the results from a very simple and effective technique for adjusting position using an aerial camera and an inertial navigation system along with ground control points. It has been demonstrated that, with sufficient targets to define straight line flight segments, the achievable position accuracy is approximately 1.5 metres horizonal or 2.2 metres total with a 1σ confidence limit. It should be noted that there is a maximum time interval between photo fixes of approximately 25 minutes, even during straight line flight segments, in order adequately to track the sinusoidal Schuler error that has a period that is approximately 84 minutes long. The concept of examining the accuracy as a function of the interval between photo fixes is only truly meaningful for the situation where the line segments are at least as long as the longest photo fix time interval. In such a situation, it would be possible to evaluate the ability of the interpolation function to track the

TABLE 2. ERROR BOUNDS (1σ) IN METERS VS AVERAGE TIME BETWEEN PHOTO FIXES

	Time interval in minutes				
Error Component	5	10	15	20	25
1 along track	2.0	3.0	13.0	57.7	97.3
2 cross track	2.5	11.3	14.5	20.4	44.3
3 altitude (barometric only)	1.6	1.6	1.6	1.8	2.0
4 horizontal (1 & 2)	3.2	11.7	19.4	61.2	107.0
5 total (1, 2 & 3)	3.5	11.8	19.5	61.2	107.0

errors of the INS. In the case of the current data set, where the average duration of the straight segments is approximately 6 minutes, any photo fix intervals greater than 6 minutes are automatically insufficient to accurately describe the flight path, and hence the perturbation in the INS error characteristics caused by changes in the flight path will not be adequately tracked by the interpolation function. In those cases where it is not possible to provide sufficient ground targets, the system performance degrades to a worst case total error of 107 metres, although the vertical error remains fairly steady throughout at 2.0 metres or less. For some applications of this technique, this may not prove to be a serious problem.

ACKNOWLEDGMENTS

The authors wish to acknowledge the continued efforts and support of the Canadian Hydrographic Service and the Canada Centre for Remote Sensing.

REFERENCES

Benson, D. O., 1975. A Comparison of Two Approaches to Pure-Inertial and Doppler-Inertial Error Analysis, *I.E.E.E. Trans. Aerospace and Electronic Systems*, Vol. AES-11, No. 4, pp 447-455.

Britting, K. R., 1971. *Inertial Navigation Systems Analysis*, Wiley Interscience, pp 15-17.

Broxmeyer, C., 1964. *Inertial Navigation Systems*, McGraw-Hill.

Masry, S. E., 1972. Measurement of Water Depth by the Analytical Plotter, presented at the 11th Annual Canadian Hydrographic Conference, Ottawa.

Masry, S. E., J. R. Gibson, A. J. D'Aoust, and D. B. Reid, 1978. Application of Inertial Navigation to Coastal Mapping, *Proceedings of the Coastal Mapping Symposium*, Rockville, Maryland, pp 17-31.

Masry, S. E., and S. MacRitchie, 1978. Different Considerations of a Universal Coastal Mapping System, *Proceedings of the International Symposium Commission IV, New Technology for Mapping.* (ISP Vol. XXII-4), Ottawa, Ontario, Canada, pp 681-701.

Savant, C. J., R. C. Howard, C. B. Solloway, and C. A. Savant, 1961. *Principles of Inertial Navigation*, McGraw-Hill.

(Received 6 October 1979; revised and accepted 24 July 1980)

Forthcoming Articles

Carlos H. Blazquez, Robert A. Elliot, and *George J. Edwards,* Vegetable Crop Management with Remote Sensing.

James B. Campbell, Spatial Correlation Effects upon Accuracy of Supervised Classification of Land Cover.

Maurice Carbonnell and *Yves Egels,* New Developments in Architectural Photogrammetry at the Institut Geographique National, France.

James B. Case, Automation in Photogrammetry.

Eugene E. Derenyi, Skylab in Retrospect.

Katherine Fitzpatrick-Lins, Comparison of Sampling Procedures and Data Analysis for a Land-Use and Land-Cover Map.

Robert B. Forrest, Simulation of Orbital Image-Sensor Geometry.

James L. Foster and *Dorothy K. Hall,* Multisensor Analysis of Hydrologic Features with Emphasis on the Seasat SAR.

C. S. Fraser and *Q. A. Abdullah,* A Simplified Mathematical Model for Applications of Analytical X-Ray Photogrammetry in Orthopaedics.

F. James Heindl, Direct Editing of Normal Equations of the Banded-Bordered Form.

Siamak Khorram, Use of Ocean Color Scanner Data in Water Quality Mapping.

V. Klemas and *W. D. Philpot,* Drift and Dispersion Studies of Ocean-Dumped Waste Using Landsat Imagery and Current Drogues.

Gottfried Konecny and *Dietmar Pape,* Correlation Techniques and Devices.

Roy A. Mead and *Patricia T. Gammon,* Mapping Wetlands Using Orthophotoquads and 35-mm Aerial Photographs.

Robert W. Merideth, Jr., Doctoral Dissertations Pertaining to Remote Sensing and Photogrammetry: A Selected Bibliography.

John C. Munday, Jr., and *Paul L. Subkoff,* Remote Sensing of Dinoflagellate Blooms in a Turbid Estuary.

P. A. Murtha and *J. A. McLean,* Extravisual Damage Detection: Defining the Standard Normal Tree.

B. J. Myers and *M. L. Benson,* Rainforest Species on Large-Scale Color Photos.

G. Petrie, Hardware Aspects of Digital Mapping.

Richard L. Threet, Stereographic Prediction of Grazing Solar Illumination.

Joseph J. Ulliman and *Oliver J. Grah,* Marking Pens for Aerial Photographs and Transparency Material.

S. W. Wharton, J. R. Irons, and *F. Huegel,* LAPR: An Experimental Pushbroom Scanner.